

Computing 3-D free surface viscoelastic flows

Xueying Xie, Matteo Pasquali

Department of Chemical Engineering, MS362

Rice University, 6100 Main St., Houston, TX 77005, USA

Abstract

Free boundary problems arise in various applications like coating, polymer processing, and biomedical engineering. In a problem with free boundaries, the physical domain is unknown a priori. Mesh generation equations must be added to the conservation equations to locate the free boundaries and map the unknown physical domain into a convenient reference one. Several mesh generation methods for free boundary problems have been developed, chiefly elliptic mesh generation and domain deformation. Whereas these methods are well-established for 2-D free boundary problems, 3-D free boundary problems still present challenges because of the sheer size of the computational problems, the complexity of 3-D free surface manipulation, and the need of using iterative solvers like GMRES [1].

This work applies domain deformation to three dimensional free boundary flows of viscoelastic liquids. The domain deformation method treats the mesh as a compressible solid. The momentum conservation equation for the elastic solid is coupled with the problem equations through appropriate boundary conditions to locate the free boundaries of the flow domain. The general conformation tensor model is used to represent the viscoelastic liquid [2]. The DEVSS-G/SUPG Finite Element method is applied to translate the differential equations of the problem into nonlinear algebraic equations. Fully coupled Newton's method with analytical Jacobian is employed to solve simultaneously the nonlinear equations for position, pressure, velocity, velocity gradient, and conformation. The restarted GMRES method with ILU preconditioner is parallelized by OpenMP to solve the large scale linear algebraic equations. The method is applied to study a model viscoelastic flow in a 3-D channel with a free surface section.

1 Introduction

Flows with free surfaces and deformable walls involve unknown boundaries, which are defined by the flow and in turn affect the flow by capillary and elastic forces. Free boundary problems arise in variety of applications like coating of polymer solutions, polymer processing, ink-jet printing, multiphase flows, blood flow in arteries, deformation of blood cells, etc. To locate the moving boundaries while computing velocity, pressure, and stress, an equation to describe the mesh must be added to the problem equations. Several methods for handling free boundary problems have been developed, chiefly elliptic mesh generation [3] and domain deformation [4]. These methods have been successful in describing 2-D free surface problems [5, 6, 7, 8, 2]. 3-D free boundary problems still present challenges because of the large scale of the computational problem and difficulty to manipulate the 3-D surface such as tangent vectors and their differentiations, especially on unstructured meshes [1, 9].

This study couples the domain deformation method to the DEVSS-G/SUPG Finite Element method to study 3-D viscoelastic flows with free boundaries. The domain deformation method treats the mesh as a compressible elastic pseudo-solid. The momentum conservation equation for the elastic pseudo-solid is coupled with all the equations of the flow to compute the shape of the domain. The general conformation tensor model is used to represent the viscoelastic liquid [2].

The mathematical formulation and the free surface boundary condition are described in Sections 2 and 3; the solution method is explained in Section 4; computational results in 2-D and 3-D free surface flows are reported in Section 5.

2 Problem formulation

This section presents the governing equations of the flow and elastic pseudo-solid (mesh), and constitutive equations. The problem equations for steady flows are

$$\mathbf{0} = \nabla \cdot \mathbf{T}^e \quad (1)$$

$$0 = \nabla \cdot \mathbf{v} \quad (2)$$

$$\mathbf{0} = \rho \mathbf{v} \cdot \nabla \mathbf{v} - \nabla \cdot \mathbf{T} - \nabla \Theta \quad (3)$$

$$\mathbf{0} = \mathbf{L} - \nabla \mathbf{v} + \frac{1}{\text{tr} \mathbf{I}} (\nabla \cdot \mathbf{v}) \mathbf{I} \quad (4)$$

$$\begin{aligned} \mathbf{0} = & \mathbf{v} \cdot \nabla \mathbf{M} - 2\zeta \frac{\mathbf{D} : \mathbf{M}}{\mathbf{I} : \mathbf{M}} \mathbf{M} - \zeta (\mathbf{M} \cdot \mathbf{D} + \mathbf{D} \cdot \mathbf{M} - 2 \frac{\mathbf{D} : \mathbf{M}}{\mathbf{I} : \mathbf{M}} \mathbf{M}) \\ & - \mathbf{M} \cdot \mathbf{W} - \mathbf{W}^T \cdot \mathbf{M} - \frac{1}{\lambda} (g_0 \mathbf{I} + g_1 \mathbf{M} + g_2 \mathbf{M}^2) \end{aligned} \quad (5)$$

Equation 1 is the momentum equation of elastic pseudo-solid for the mesh, eqn.2 is the continuity equation, eqn.3 is the momentum equation, eqn.4 is the velocity gradient interpolation equation used to improve the stability and convergence of the computational method [2, 7], and eqn.5 is the conformation transport equation.

\mathbf{T}^e is the Cauchy stress tensor of the elastic pseudo-solid, \mathbf{v} is the velocity, ρ is the density, Θ is the potential of body force per unit volume, \mathbf{T} is the stress tensor, \mathbf{L} is the velocity gradient, \mathbf{M} is the conformation tensor, ξ and ζ are the polymer resistance to stretching and orientation, λ is the relaxation time, g_0 , g_1 , and g_2 define the rate of relaxation of the polymer segments [2, 7, for details].

The stress in an elastic solid is [10],

$$\mathbf{T}^e = 2\rho\mathbf{B} \cdot \frac{\partial w}{\partial \mathbf{B}} \quad (6)$$

where $\rho \sim \frac{1}{\sqrt{\mathbb{I}_B}}$, $\mathbf{B} = \mathbf{F}^d \cdot \mathbf{F}^{dT}$ is the left Cauchy-Green tensor or Finger tensor, \mathbf{F}^d is the deformation gradient with $F_{ij}^d = \frac{\partial x_i}{\partial x_{0j}}$, \mathbf{x}_0 is the referential physical position, \mathbf{x} is the current physical position; w is stored energy, and its derivative with respect to \mathbf{B} is $\frac{\partial w}{\partial \mathbf{B}} = \frac{\partial w}{\partial I} \frac{\partial I}{\partial \mathbf{B}} + \frac{\partial w}{\partial II} \frac{\partial II}{\partial \mathbf{B}} + \frac{\partial w}{\partial III} \frac{\partial III}{\partial \mathbf{B}}$, where $\frac{\partial I}{\partial \mathbf{B}} = \mathbf{I}$, $\frac{\partial II}{\partial \mathbf{B}} = \mathbf{II} - \mathbf{B}$, and $\frac{\partial III}{\partial \mathbf{B}} = \mathbb{III}\mathbf{B}^{-T}$. I , II , and III are the first, the second, and the third invariants of \mathbf{B} respectively. Thus,

$$\mathbf{T}^e = \frac{2}{\sqrt{\mathbb{I}_B}} \left[\left(\mathbb{I}_B \frac{\partial w}{\partial \mathbf{B}} + \mathbb{II}_B \frac{\partial w}{\partial \mathbf{B}} \right) \mathbf{I} + \frac{\partial w}{\partial I_B} \mathbf{B} - \mathbb{III}_B \frac{\partial w}{\partial \mathbf{B}} \mathbf{B}^{-1} \right] \quad (7)$$

A compressible neo-Hookean free energy is used to control the mesh [8]

$$w = aI + cIII - d \log_{10} \sqrt{III} \quad (8)$$

where $a = 1$, $c = 1/3$ and $d = 8 \ln 10/3$.

The conformation tensor describes the flow-induced distortion of polymer coils. The eigenvectors of \mathbf{M} represent the principal directions along which the polymer chains are stretched, contracted, or oriented. The eigenvalues of \mathbf{M} represent the square of the principal stretch ratios. The details of the conformation tensor and its evolution equation are described in Refs. [2, 7, 11].

The stress \mathbf{T} can be split into 3 parts,

$$\mathbf{T} = -p\mathbf{I} + \boldsymbol{\tau} + \boldsymbol{\sigma} \quad (9)$$

where p is the pressure, $\boldsymbol{\tau}$ is the viscous stress,

$$\boldsymbol{\tau} = 2\mu\mathbf{D} = \mu(\nabla\mathbf{v} + \nabla\mathbf{v}^T) \quad (10)$$

$\boldsymbol{\sigma}$ is the elastic stress which follows the constitutive relation [7]

$$\underbrace{\boldsymbol{\sigma}}_{\substack{\text{elastic} \\ \text{stress}}} = 2\rho\xi \underbrace{\frac{\mathbf{M}}{\mathbf{I}:\mathbf{M}} \mathbf{M} : \frac{\partial a}{\partial \mathbf{M}}}_{\substack{\text{stress by} \\ \text{molecular stretching}}} + 2\rho\zeta \underbrace{\left(-\frac{\mathbf{M}}{\mathbf{I}:\mathbf{M}} \mathbf{M} : \frac{\partial a}{\partial \mathbf{M}} + \mathbf{M} \cdot \frac{\partial a}{\partial \mathbf{M}} \right)}_{\substack{\text{stress by molecular orientation}}} \quad (11)$$

where $a(\mathbf{M})$ is the Helmholtz free energy per unit volume of the polymer liquid.

3 Boundary conditions at free interfaces

Boundary conditions at free interfaces present computational challenges. The velocity is continuous across the interface, whereas other quantities like pressure, stress, velocity gradient, and conformation can be discontinuous. The kinematic boundary condition $\mathbf{n} \cdot \mathbf{v} = 0$ enforces the immiscibility of the materials on the two sides.

3.1 Boundary conditions on the mesh equations

In the normal direction to the boundary, the kinematic condition determines the position of an interface

$$\mathbf{n} \cdot \mathbf{v} = 0 \quad (12)$$

This condition is imposed essentially, i.e., it replaces the normal mesh equation on the boundary nodes.

In the domain deformation method, the tractions in the tangent directions determine the node distribution on the surface. For simplicity, zero traction can be imposed to achieve uniform nodal distribution,

$$\mathbf{t}\mathbf{n} : \mathbf{T}^e = 0 \quad (13)$$

In a 2-D problem, this boundary condition is enforced by replacing the tangential mesh equation with it. In a 3-D problem, calculating the derivative of tangent vectors on unstructured meshes is difficult; thus, the mesh equations are rotated into two tangent directions and the boundary condition is easily imposed through the boundary integral of the traction, which is zero. For simplicity, the residual and Jacobian matrix are rotated after the integration [1]. In 3-D, there are countless tangent directions; at every node on the boundary, the unit tangent vectors are usually different when they are calculated from different elements. However, the normal direction coincides within numerical error. In order to obtain two orthogonal unit tangent vectors consistent for one node in all elements, the tangent vectors at every node are computed globally. At every node, the unit normal vector \mathbf{n} is averaged from all the neighboring elements. The first unit tangent vector is calculated by

$$\mathbf{t}_1 = \frac{(\mathbf{I} - \mathbf{n}\mathbf{n}) \cdot \mathbf{s}}{\|(\mathbf{I} - \mathbf{n}\mathbf{n}) \cdot \mathbf{s}\|} \quad (14)$$

where \mathbf{s} is the seed vector [1]. \mathbf{s} is chosen from a tangent vector calculated at the node in a neighboring element. The second unit tangent is calculated by

$$\mathbf{t}_2 = \mathbf{n} \times \mathbf{t}_1 \quad (15)$$

3.2 Momentum boundary conditions

The dynamic equilibrium of the interface sets the boundary conditions on the momentum equation,

$$\mathbf{n}_1 \cdot (\mathbf{T}_1 - \mathbf{T}_2) = \nabla_{\mathcal{I}} \cdot \mathbf{\Pi} \quad (16)$$

where 1 and 2 denote the two sides of the interface, \mathbf{n}_1 is the unit normal vector on the interface directed from 1 to 2—hereafter $\mathbf{n} = \mathbf{n}_1$. The surface gradient is $\nabla_{\mathcal{I}} \equiv (\mathbf{I} - \mathbf{nn}) \cdot \nabla$, and $\mathbf{\Pi}$ is the surface stress which depends on the property of the interface or membrane. For a liquid-liquid or liquid-gas interface, $\mathbf{\Pi} = \gamma(\mathbf{I} - \mathbf{nn})$, where γ is the surface tension; for a general membrane [12],

$$\mathbf{\Pi} = 2(I_2 + 1)^{\frac{1}{2}} \frac{\partial W}{\partial I_2} (\mathbf{I} - \mathbf{nn}) + 2(I_2 + 1)^{-\frac{1}{2}} \frac{\partial W}{\partial I_1} \mathbf{A} \quad (17)$$

where W is the surface strain energy function, $\mathbf{A} \equiv (\mathbf{I} - \mathbf{nn}) \cdot \mathbf{B} \cdot (\mathbf{I} - \mathbf{nn})$ is the symmetric surface Cauchy-Green strain tensor, with invariants $I_1 = \text{tr} \mathbf{A} - 2$ and $I_2 = \frac{1}{2}(\text{tr}(\mathbf{A})^2 - \text{tr}(\mathbf{A}^2)) - 1$. When $W = \gamma(I_2 + 1)^{\frac{1}{2}}$, $\mathbf{\Pi} = \gamma(\mathbf{I} - \mathbf{nn})$. If γ is constant, $\nabla_{\mathcal{I}} \cdot \mathbf{\Pi} = -\gamma \mathbf{n} \nabla_{\mathcal{I}} \cdot \mathbf{n}$. If on side two there is a gas with negligible viscous stress, then $\mathbf{n} \cdot \mathbf{T} = -p\mathbf{n} + \nabla_{\mathcal{I}} \cdot \mathbf{\Pi}$. If the free boundary is a membrane, the tangential components of the liquid velocity vanish; in this case, the two tangential components of the momentum equation are replaced by the no-slip condition, whereas the normal component of the momentum equation obeys the dynamical condition 16.

4 Solution method

The DEVSS-G/SUPG Finite Element Method is applied to reduce the partial differential equations of the flow to algebraic equations. In 2-D problems, 9-node quadrilateral elements are used. Velocity and position basis functions are biquadratic and continuous, velocity gradient, conformation basis functions are bilinear and continuous, and pressure basis functions are linear and discontinuous. In 3-D problems, 10-node tetrahedral elements are used. The basic functions for velocity and position are quadratic and continuous, those for pressure, velocity gradient and conformation are linear and continuous. The set of nonlinear algebraic equations is solved by the fully coupled Newton's method with analytical Jacobian, which yields a large scale linear algebraic system $\mathbf{J}\Delta\mathbf{x} = \mathbf{R}$, where \mathbf{J} is the Jacobian matrix, $\Delta\mathbf{x}$ is the Newton update, and \mathbf{R} is the residual vector. A frontal solver, parallelized by OpenMP is employed to solve the linear system in 2-D flows. Restarted GMRES with ILU preconditioner parallelized by OpenMP is used in 3-D flows. The code runs on an IBM Regatta with 64 GB shared memory and 16 1.33 GHz Power4 processors.

5 Results

The method is applied to compute two 2-D steady flows and one 3-D flow.

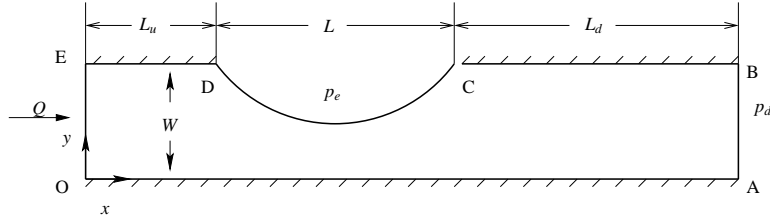


Figure 1: Geometry of the 2-D collapsible channel; the segment DC is an elastic membrane wall.

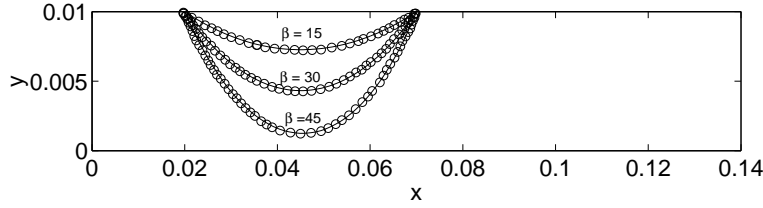


Figure 2: Deformed wall shape with steady flow in the 2-D collapsible channel, obtained at $Re = 1$, $p_d^* = 9.3 \times 10^4$, and $\gamma^* = \gamma_0^*/\beta$. The solid line denotes the results of this study, the open symbols are the results of Ref. [13].

5.1 2-D membrane in collapsible channel

Fig. 1 shows a 2-D channel with a segment of the wall replaced by an elastic membrane. This steady flow in the 2-D collapsible channel is chosen for checking the boundary condition for membrane by comparing the numerical results with those reported in Ref. [13]. This case describes a flow that occurs in some physiological applications such as aneurysm in the body.

In the collapsible channel, no-slip is imposed at rigid walls; the membrane segment is assumed to be elastic. Following [13], the membrane is taken to have a simple constitutive equation, $\Pi = \gamma(\mathbf{I} - \mathbf{nn})$. A fully developed velocity profile is imposed on the inflow boundary, i.e., $\mathbf{v} = \mathbf{v}(\mathbf{x})$. At the outflow, the flow is fully developed and the pressure is fixed, i.e., $\mathbf{n} \cdot \nabla \mathbf{v} = \mathbf{0}$ and $p = p_d$. The deformations of the elastic segment with different constant membrane rigidity are shown in Fig.2 under the conditions: $Re \equiv \rho Q/\mu = 1$, $p_d^* \equiv (p_e - p_d)W^2\rho/\mu^2 = 9.3 \times 10^4$, $\gamma^* = \gamma_0^*/\beta$ (with $\beta = 15, 30, 45$ and $\gamma_0^* \equiv \gamma_0 W\rho/\mu^2 = 1.610 \times 10^7$). In units of W , the dimensions of the channel are $L_u^* \equiv L_u/W = 2$, $L^* \equiv L/W = 5$, $L_d^* \equiv L_d/W = 7$. Fig. 2 shows that the results are in excellent agreement with those of Ref. [13].

5.2 Free surface and interfacial flow in slot coater

The flow in the downstream section of a slot coater is computed in two different ways: as the flow of a liquid with a free surface and as the flow of a liquid and a

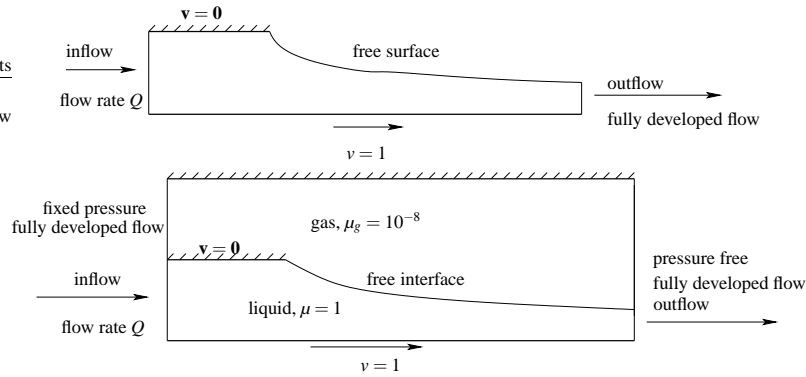


Figure 3: Flow in the downstream of the slot coater: free surface model (top) and interfacial model (bottom).

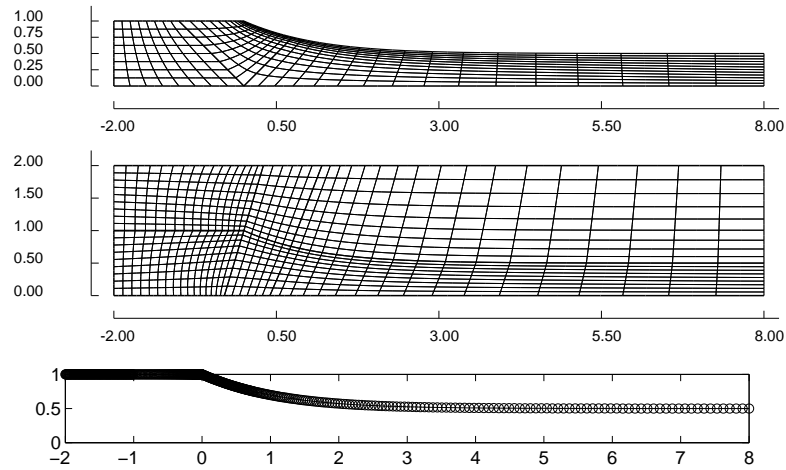


Figure 4: Meshes and free surfaces computed as part of solutions. $Q = 0.5$, $Re = 0$, $Ca = 0.1$. The open symbols and the solid line denote the results from free surface model and interfacial model respectively.

low-viscosity gas coupled at an interface (Fig. 3).

Both flows are computed at $Q \equiv 0.5hv$, $Re \equiv \rho vL/\mu = 0$, $Ca \equiv \mu v/\gamma = 0.1$. Here Q is the flow rate per unit width of the slot, h is the gap, v is the velocity of the bottom wall, μ is the liquid viscosity, and γ is the surface tension. Fig. 4 shows the meshes computed by solving the flow of a single liquid and that of two fluids; in the latter case, the viscosity of the gas is set to $\mu_g = 10^{-8}\mu$. The free surface computed with the two methods is the same; thus, the method for computing the interfacial flow is correct.

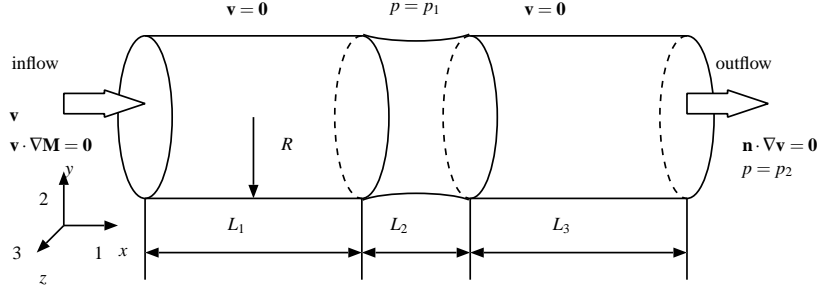


Figure 5: 3-D collapsible cylindrical channel and boundary conditions. $R = 1$, $L_1 = L_3 = 1$, $L_2 = 0.5$.

5.3 Viscoelastic flow in a 3-D channel with a free surface section

The flow of an Oldroyd-B liquid in a 3-D channel with a free surface section is chosen to test the method. The parameters in the conformation transport equation are $\xi = 1$, $\zeta = 1$, $g_0 = -1$, $g_1 = 1$, $g_2 = 0$, and $\frac{\partial a}{\partial \mathbf{M}} = \frac{G}{2p} \mathbf{I}$, where $G = \frac{\eta_p}{\lambda}$ is the polymer modulus and η_p is the polymer viscosity.

The dimensions of the channel and the boundary conditions are shown in Fig. 5. The computation is carried out on three meshes at $Q = 0.5$, $\Delta p = 31.42$, $Re \equiv \rho Q / (\pi R \mu) = 0$, $Ca \equiv \mu Q / (\pi R^2 \gamma) = 0.080$ to 0.122 , and $Wi \equiv 4Q\lambda / (\pi R^3) = 0.064$ to 1.019 . Here Q is the flow rate, $\Delta p \equiv (p_1 - p_2)\pi R^3 / (\mu Q)$, and μ is the total viscosity of the solvent and polymer. The polymer viscosity is $\eta_p = 0.41\mu$. Mesh 1 is a coarse mesh (2,493 elements, 33,342 unknowns); mesh 2 is finer at the free surface and coarse at the inflow and outflow (2,895 elements, 39,470 unknowns); mesh 3 is the finest (8,092 elements, 100,434 unknowns). Fig. 6 shows the computed free surface mesh and the contours of axial component of the conformation tensor M_{11} on mesh 3 at $Ca = 0.122$ and $Wi = 0.637$. The polymer chains are stretched under the upstream section of the free surface, where the liquid accelerates, then contract in the downstream section as the liquid decelerates. The computed free surfaces at the $y = 0$ plane are shown in Fig. 7 on the three meshes at different capillary and Weissenberg numbers. The plot shows that the shapes of the free surfaces computed on the three meshes match very well under the same conditions; the shapes change with capillary number and Weissenberg number. As the value of capillary number grows, the free surface deforms further. The two curvatures in 3-D partly cancel in this case because they have opposite signs. At $Ca = 0.106$ and $Wi = 0.064$, the longitudinal curvature radius is ≈ -0.33 , whereas the circumferential curvature radius is ≈ 0.87 ; thus, the longitudinal curvature dominates and the free surface deforms more with increasing capillary number as shown in Fig. 7. As Weissenberg number increases, the free surface deforms less because the stretched polymer develops compressive elastic stresses normal to the free surface, which resist the deformation of the free surface.

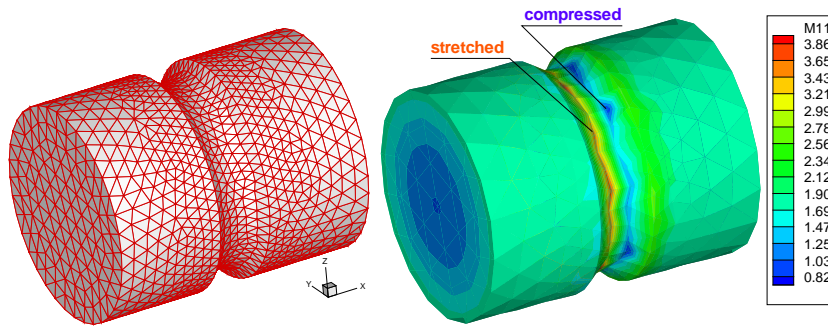


Figure 6: Computed free surface mesh and contours of the axial component of the conformation tensor M_{11} in a 3-D cylindrical channel with a collapsible section. $Ca = 0.122$ and $Wi = 0.637$.

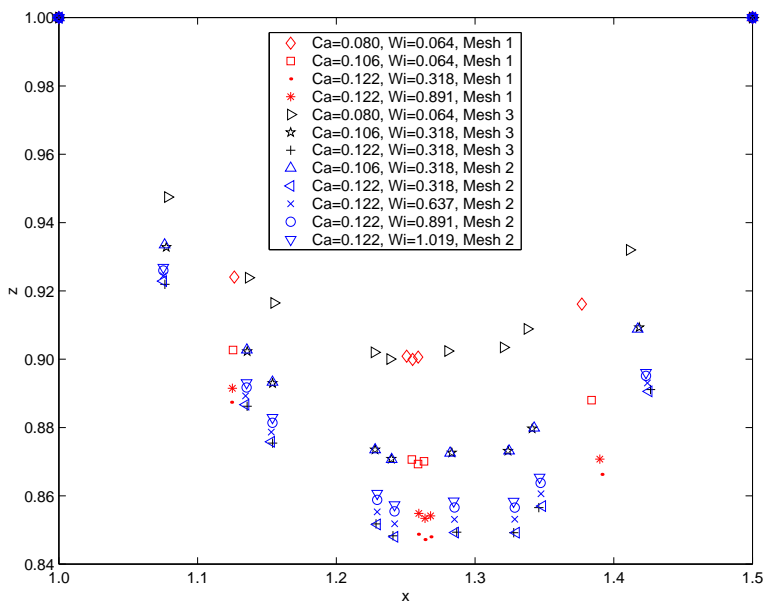


Figure 7: Computed free surface at the $y = 0$ plane of the 3-D channel at different capillary and Weissenberg numbers.

6 Conclusion

The domain deformation method coupled with DEVSS-G/SUPG Finite Element method is applied to compute free surface flows. This method is validated against published literature [13] in a 2-D flow in a channel with a deformable membrane on one wall, and by comparing a free surface flow from the literature with a flow at

a gas-liquid interface where the gas viscosity is vanishingly small. In both cases, excellent agreement is found. Finally, computational results are presented on viscoelastic flow of an Oldroyd-B liquid in a 3-D channel with a free surface section.

Acknowledgments

The authors thank M. Behr, L. Musson, K. Zygourakis, and D. Sorensen for useful discussions. The work was partially supported by the National Science Foundation (CTS-CAREER-0134389) and by a gift from ExxonMobil. A color version of the article is at <http://www.ruf.rice.edu/~mp/articles/wit2003-3Dvefreesurface.pdf>.

References

- [1] Cairncross, R.A., Schunk, P.R., Baer, T.A., Rao, R.R. & Sackinger, P.A., A finite element method for free surface flows of incompressible fluids in three dimensions. part i. boundary fitted mesh motion. *Int J Numer Meth Fluids*, **33**, pp. 375–403, 2000.
- [2] Pasquali, M. & Scriven, L.E., Free surface flows of polymer solutions with models based on the conformation tensor. *J Non-Newton Fluid Mech*, **108**, pp. 363–409, 2002.
- [3] Christodoulou, K.N. & Scriven, L.E., Discretization of free surface flows and other moving boundary problems. *J Comp Phys*, **99**, pp. 39–55, 1992.
- [4] Sackinger, P.A., Schunk, P.R. & Rao, R.R., A Newton-Raphson pseudo-solid domain mapping technique for free and moving boundary problems: A finite element implementation. *J Comput Phys*, **125**, pp. 83–103, 1996.
- [5] de Almeida, V.F., *Gas-Liquid Counterflow through Constricted Passages*. Ph.D. thesis, University of Minnesota, Minneapolis, MN, 1995.
- [6] Carvalho, M.S., *Roll Coating Flows in Rigid and Deformable Gaps*. Ph.D. thesis, University of Minnesota, Minneapolis, MN, 1996.
- [7] Pasquali, M., *Polymer Molecules in Free Surface Coating flows*. Ph.D. thesis, University of Minnesota, 2000.
- [8] Musson, L.C., *Two-layer Slot Coating*. Ph.D. thesis, University of Minnesota, 2001.
- [9] Hooper, R.W., *Drop Dynamics in Polymer Processing Flows*. Ph.D. thesis, University of Minnesota, 2001.
- [10] Başar, Y. & Weichert, D., *Nonlinear Continuum Mechanics of Solids*. Springer: New York, 1st edition, 2000.
- [11] Beris, A.N. & Edwards, B.J., *Thermodynamics of Flowing Systems with Internal Microstructure*. Oxford University Press: Oxford, 1st edition, 1994.
- [12] Pozrikidis, C., Finite deformation of liquid capsules enclosed by elastic membranes in simple shear flow. *J Fluid Mech*, **297**, pp. 123–152, 1995.
- [13] Luo, X.Y. & Pedley, T.J., A numerical simulation of steady flow in a 2-d collapsible channel. *J Fluid Struct*, **9**, pp. 149–184, 1995.